Journal of Environmental Chemical Engineering 14 (2026) 120742

Contents lists available at ScienceDirect

Journal of Environmental Chemical Engineering

journal homepage: www.elsevier.com/locate/jece

Synergistic one-step pyrolysis of waste coffee grounds and orange peels: A green route to hierarchical porous carbon for high-performance supercapacitors

Yu-Cheng Chang *, Shao-Ru Chang

Department of Materials Science and Engineering, Feng Chia University, Taichung 40724, Taiwan

ARTICLE INFO

Keywords:
Electrode Materials
Biowaste
Coffee Grounds
Orange Peels
Natural Activating Agent

ABSTRACT

The development of sustainable, low-cost electrode materials from biowaste is critical for advanced energy storage. Herein, we report a green and scalable one-step co-pyrolysis strategy for synthesizing high-performance porous carbon from waste coffee grounds (CF) as the precursor and orange peels (OP) as a natural activating agent. Through systematic optimization of parameters—including pyrolysis temperature, CF: OP mass ratio, and coffee roast level—an optimal synthesis route was established. The optimized material (CFOP), prepared at 800 °C with a 1: 1 mass ratio of light-roast CF and OP, exhibited a high specific capacitance of 275.3 F/g at a current density of 1 A/g. Structural analysis confirmed that the synergistic in-situ activation of OP and residual potassium generated a hierarchical porous architecture with improved graphitization and electrical conductivity, both essential for enhanced electrochemical performance. Kinetic studies revealed a diffusion-dominated pseudocapacitive storage mechanism. Furthermore, the CFOP electrode demonstrated excellent long-term cycling stability, maintaining 63.27 % of its initial capacitance after 5000 cycles with a high coulombic efficiency of 97.29 %. This work presents a facile route to convert agricultural waste into a valuable electrode material, highlighting its significant potential for practical energy storage applications.

1. Introduction

The rapid evolution of technology, while significantly enhancing daily life, has precipitated critical challenges related to the accelerated depletion of fossil fuels and consequent environmental degradation [1,2]. The finite nature and inequitable global distribution of these resources underscore the need to develop renewable energy sources and corresponding energy storage solutions [3,4]. Consequently, mitigating environmental pollution and addressing the escalating energy crisis have become paramount scientific and societal objectives [5,6]. To harness intermittent renewable energy sources effectively, the development of efficient energy storage devices and systems is indispensable [7,8]. Among various energy storage technologies, supercapacitors, also known as electrochemical capacitors, have attracted considerable attention [9]. They occupy a unique niche between conventional batteries and dielectric capacitors, offering a compelling combination of high power density, rapid charge/discharge kinetics, exceptional cycling stability, and inherent safety [10,11]. However, a primary limitation of supercapacitors is their comparatively lower energy density relative to batteries [12,13]. A central challenge in the field is the strategic design and selection of advanced materials to fabricate high-performance supercapacitors that concurrently exhibit high energy and power densities [14,15]. Enhancing these key performance metrics is crucial for expanding their utility, enabling their deployment as standalone power sources or in hybrid configurations with batteries to broaden their application scope [16,17].

To address the growing demand for high-performance electrode materials, numerous synthesis strategies have been explored for producing porous carbon [18]. Globally, the development of hierarchical porous carbons (HPCs) has become a focal point for high-performance supercapacitors due to their ability to facilitate rapid ion transport and provide accessible active sites [19,20]. Current-state-of-the-art HPCs derived from various synthetic and biomass precursors typically exhibit specific capacitances of 150–250 F/g in aqueous electrolytes [21–23]. However, achieving these high-performance metrics often necessitates complex synthesis routes. Template-assisted synthesis, which employs sacrificial scaffolds such as silica or metal oxides, enables precise control over pore architecture; however, it introduces additional

* Corresponding author.
E-mail address: yuchchang@fcu.edu.tw (Y.-C. Chang).

https://doi.org/10.1016/j.jece.2025.120742
Received 22 October 2025; Received in revised form 22 November 2025; Accepted 15 December 2025
Available online 15 December 2025
2213-3437/© 2025 Elsevier Ltd. All rights are reserved, including those for text and data mining, AI training, and similar technologies.

processing steps and increases production cost [24]. Meanwhile, several advanced fabrication techniques—including thermal plasma carbonization, microwave-assisted pyrolysis, and electrochemical activation—have emerged as efficient alternatives, offering rapid heating rates and improved kinetic control [25,26]. Despite these advances, the sustainable and scalable production of porous carbon remains a key challenge [27].

In this context, valorizing abundant biomass waste as a carbon precursor offers an attractive pathway, providing environmental benefits, reduced reliance on hazardous chemicals, and economic feasibility for large-scale manufacturing [28–30]. For instance, spent coffee grounds (CF), a significant byproduct of global coffee consumption, are a rich source of caffeine, proteins, minerals, and other value-added organic compounds, imparting them with diverse chemical functionalities [31–33]. Through thermochemical treatments, such as carbonization and subsequent activation, these precursors can be converted into porous biochar, which exhibits a highly developed porous structure and substantially enhanced electrochemical properties, making it suitable for energy storage applications [34,35]. Similarly, orange peels (OP), a prevalent byproduct of the citrus industry, are another promising feedstock [36]. Its composition, rich in cellulose, hemicellulose, pectin, and various mineral elements, including nitrogen, makes it an abundant and low-cost resource [37]. Notably, carbon derived from orange peel can not only improve charge storage capacity in electrochemical devices but also serve as a green activating agent, potentially replacing conventional, often harsh chemical activators [38,39]. Leveraging the unique physicochemical characteristics of these waste-derived precursors, the resulting carbon materials are being extensively explored for applications in supercapacitors, dye adsorption, and biofuel production, thus offering significant environmental and economic advantages [40,41].

Biochar, the solid product obtained from the pyrolysis or thermal treatment of biomass, has emerged as a promising functional material [42,43]. It is distinguished by several advantageous characteristics, including its eco-friendly nature, low production cost, high specific surface area, and a well-developed porous network [44]. The inherent physical properties and diverse chemical composition of the precursor biomass, which often contains various microstructures and heteroatoms, facilitate the in-situ doping of the resulting biochar [45,46]. This self-doping introduces heteroatoms into the carbon lattice, generating additional active sites for ion adsorption and enhancing the electrode surface's electrolyte wettability [47,48]. Despite these merits, the intrinsic hydrophobicity and the prevalence of micropores in pristine biochar can limit the efficient transport of electrolyte ions, thereby constraining electrochemical performance [49,50]. To address this challenge, significant research efforts are directed towards tailoring the pore structure. The implementation of optimized carbonization and activation methodologies is crucial for engineering a hierarchical porous architecture, which effectively facilitates rapid ion diffusion and transport, ultimately enhancing the material's capacitive performance [20,51].

Therefore, the primary objective of this study is to develop a green, scalable, and cost-effective route for synthesizing high-performance electrode materials by exploiting the synergistic interaction between two abundant biowastes. The novelty of this work lies in the strategic use of orange peels (OP) not merely as a carbon source, but as a natural, in-situ activating agent for spent coffee grounds (CF) via a one-step co-pyrolysis process. This approach eliminates the need for corrosive chemical activators while simultaneously inducing a hierarchical porous architecture. Specifically, we aim to optimize the synthesis parameters—including pyrolysis temperature and precursor mass ratio—to maximize electrochemical performance. Furthermore, this study seeks to elucidate the underlying charge-storage mechanism and to demonstrate the practical viability of the optimized CFOP materials through rigorous kinetic analysis and long-term stability testing.

2. Experimental

2.1. Chemicals and materials

Spent coffee grounds and orange peels were collected from local coffee shops and supermarkets. These biomass precursors were thoroughly washed with deionized (DI) water, oven-dried, and subsequently ground into fine powders for subsequent use. Commercial carbon black was obtained from Cabot Corporation and used as received. Polyvinylidene fluoride (PVDF, $-(C_2H_2F_2)_n-$, 100 %) was supplied by Scientific Polymer Products, Inc., while 1-methyl-2-pyrrolidone (NMP, C_5H_9NO, 99.5 %) was purchased from Echo Chemical Co., Ltd. Potassium hydroxide (KOH, 85 %) and hydrochloric acid (HCl, 37 wt% aqueous solution) were provided by Showa Chemical Co., Ltd. and Aencore, respectively. Acetone (CH_3COCH_3, 99 %) and ethanol (C_2H_5OH, 95 %) were obtained from Jingming Chemical Co., Ltd. All chemical reagents were of analytical grade and used without further purification. Deionized water was used throughout all solution preparations.

2.2. Preparation of coffee grounds and orange peels

The waste coffee grounds and orange peels underwent a systematic pre-treatment process. The coffee grounds were thoroughly washed multiple times with deionized (DI) water and filtered to eliminate residual impurities. For the orange peels, fresh oranges were rinsed with DI water, and the outer colored layer (flavedo) was carefully separated. Both the purified coffee grounds and collected flavedo were dried in a convection oven at 75 °C for 12 h. The dried materials were then subjected to a two-stage grinding process: initially pulverized using a mortar and pestle, followed by further milling with a manual grinder to obtain fine, homogeneous powders. The resulting precursor powders were stored in a desiccator for subsequent use.

2.3. Synthesis of coffee ground and orange peel-derived carbon (CFOP)

The as-prepared coffee ground and orange peel powders, as detailed in Section 2.1, were thoroughly mixed at a 1:1 mass ratio to obtain a homogeneous precursor blend. This mixture was then carbonized in a tubular furnace. The sample was heated from room temperature to 800 °C at a constant rate of 5 °C/min under a continuous nitrogen (N_2) flow to ensure an inert atmosphere. Upon reaching the target temperature, the sample was maintained at different pyrolysis temperatures for 2 h. Thermogravimetric analysis (Figure S1) was utilized to characterize the thermal decomposition behavior of CFOP materials during high-temperature pyrolysis, thereby informing the selection of appropriate thermal annealing temperatures. Specifically, pyrolysis temperatures of 400, 600, and 800 °C were chosen to systematically investigate the impact of increasing carbonization severity and to ensure adequate removal of residual organic matter [52]. Following the heat treatment, the furnace was allowed to cool naturally to ambient temperature. The resulting product was thoroughly washed with deionized water and ethanol, separated by centrifugation, and subsequently dried at 70 °C for 2 h. The resulting black carbonaceous solid was collected and designated as CFOP.

2.4. Materials characterization

The microstructural characteristics of the materials were investigated using field-emission scanning electron microscopy (FE-SEM, Hitachi S-4800) and transmission electron microscopy (TEM, JEOL JEM-2100F). Elemental composition and spatial distribution were analyzed through energy-dispersive X-ray spectroscopy (EDS, Oxford Instruments X-MAX). Molecular structure identification was performed using a multi-functional micro-Raman spectrometer (MRI series). Additionally, the crystallinity and phase structure of the samples were examined using

X-ray diffraction (XRD, Bruker D2 Phaser).

2.5. Electrochemical measurements

Prior to electrochemical testing, nickel foam substrates underwent a sequential cleaning process. The substrates were ultrasonicated for 10 min each in hydrochloric acid, acetone, ethanol, and deionized (DI) water to remove surface impurities, followed by drying in an oven at 75 °C overnight. The electrode slurry was prepared by thoroughly mixing the active material (CFOP), carbon black, and polyvinylidene fluoride (PVDF) in a weight ratio of 8:1:1. An appropriate amount of N-methyl-2-pyrrolidone (NMP) was added to obtain a uniform slurry, which was subsequently sonicated for 30 min. A volume of 75 μL of the resulting slurry was then drop-cast onto the cleaned nickel foam and dried at 50 °C overnight, following procedures reported in the literature [15]. Electrochemical measurements were performed using a specialized electrochemical workstation (Zahner Zennium), equipped with high-precision impedance and potentiostatic/galvanostatic modules suitable for three-electrode analysis. The prepared CFOP electrode served as the working electrode, a saturated calomel electrode (SCE) as the reference, and a platinum foil as the counter electrode. All tests were conducted in an aqueous 3 M KOH electrolyte.

3. Results and discussion

3.1. Optimization of biomass precursor carbonization

To establish a foundation for the development of advanced electrode materials, the carbonization behaviors of the individual biomass precursors—waste coffee grounds (CF) and orange peel (OP)—were systematically investigated. This initial investigation was essential for understanding the intrinsic properties of the biomass precursors and determining the optimal pyrolysis temperature based on the relationship between their evolving microstructure and electrochemical performance. The morphological changes with increasing carbonization temperature were first examined by field-emission scanning electron microscopy (FESEM). As shown in Fig. 1, the coffee grounds exhibited notable structural consolidation upon thermal treatment. With increasing pyrolysis temperature from 400 °C to 800 °C, the initially porous framework gradually transformed into a denser and less porous matrix. In particular, the sample carbonized at 800 °C (800CF) displayed the most compact morphology. Such densification is typically attributed to the thermal shrinkage and fusion of carbonaceous matter during pyrolysis. However, excessive compactness may hinder electrolyte ion diffusion by forming tortuous transport pathways, thereby reducing the accessibility of electrochemically active sites and ultimately impairing overall performance [53,54]. In sharp contrast, the orange peel (OP) precursor exhibited an opposing morphological trend, as shown in Fig. 2. Increasing the carbonization temperature led to the volatilization of organic constituents, resulting in gas evolution that generated a progressively more intricate and well-developed porous structure. This effect was most pronounced in the OP-800 sample, which exhibited a highly porous architecture that facilitated efficient electrolyte infiltration and an enlarged electrode–electrolyte interface. To further investigate structural transformations at the atomic level, Raman spectroscopy was performed (Figures S2 and S3). For both CF and OP samples, the intensity ratio of the D band (~1348 cm^{-1}, indicative of structural disorder and defects) to the G band (~1591 cm^{-1}, corresponding to the in-plane vibrations of sp^2-hybridized graphitic carbon) increased with rising pyrolysis temperature. Specifically, the I_D/I_G ratios for CF-400, CF-600, and CF-800 were 0.452, 0.666, and 0.808, respectively. Those for OP-400, OP-600, and OP-800 were 0.471, 0.608, and

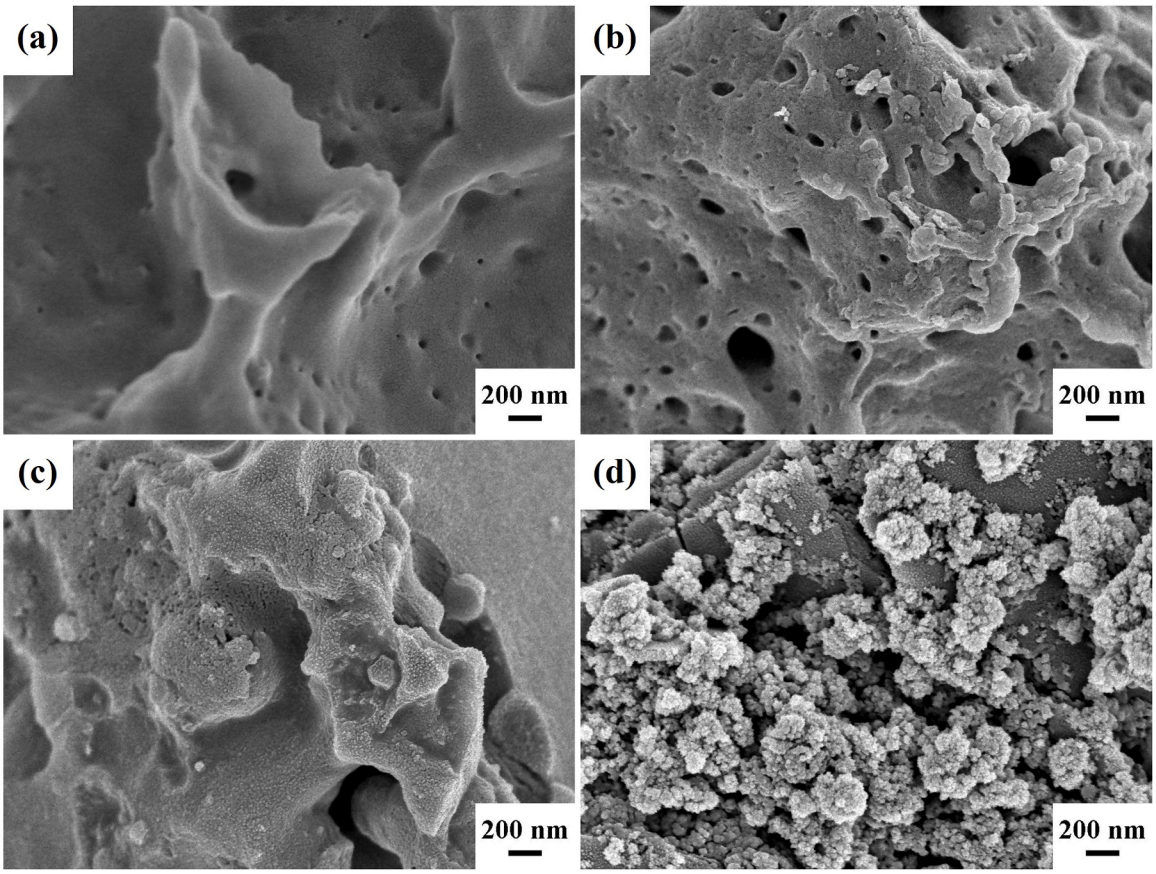


Fig. 1. The FESEM images of coffee grounds (CF) before and after carbonization at various temperatures: (a) raw coffee grounds; (b) CF-400 (400 °C); (c) CF-600 (600 °C); (d) CF-800 (800 °C).

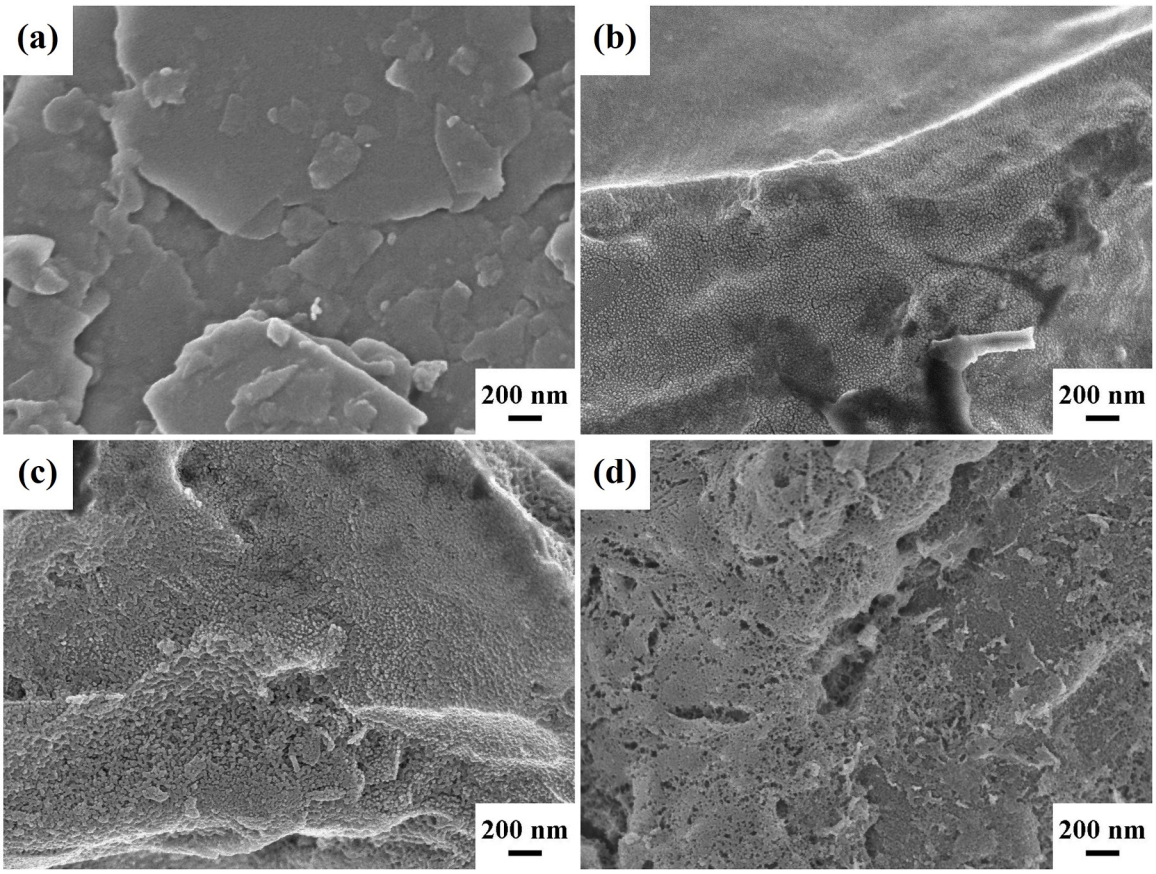


Fig. 2. The FESEM images of orange peels (OP) before and after carbonization at different temperatures: (a) raw orange peels; (b) OP-400 (400 °C); (c) OP-600 (600 °C); (d) OP-800 (800 °C).

0.762, respectively. This increasing trend suggests that higher carbonization temperatures within this range promoted the fragmentation of extended sp^2 domains and the formation of additional edge sites and lattice defects, rather than enhancing graphitization [55,56]. Although indicative of disorder, such structural defects can be advantageous, as they provide abundant electrochemically active sites favorable for charge storage.

To assess the electrochemical characteristics of the CF prepared at different temperatures, cyclic voltammetry (CV) was employed, as illustrated in Fig. 3a-b. The CV profiles for all CF samples exhibit prominent redox peaks, indicating that charge storage is primarily governed by a diffusion-controlled pseudocapacitive mechanism rather than by electric double-layer capacitance (EDLC). Notably, the CF-600 electrode exhibited the largest integrated CV area (Fig. 3a), achieving a peak specific capacitance of 219.7 F/g at a scan rate of 5 mV/s. This performance notably exceeds that of the CF-800 (178.2 F/g) and CF-400 (106.4 F/g) samples. These findings are corroborated by galvanostatic charge–discharge (GCD) analysis (Fig. 3b), which shows characteristic Faradaic potential plateaus. Consistent with the CV data, the CF-600 sample demonstrated the most prolonged discharge duration, resulting in a specific capacitance of 141.8 F/g at a current density of 1 A/g. The inferior performance of the CF-800 sample is attributed to its highly densified microstructure, which restricts electrolyte infiltration, as well as a high concentration of defects that likely impedes efficient electron transport.

A parallel evaluation was conducted for the orange peel-derived carbons (OP), with the verified data presented in Fig. 3c and 3d. Similar to the CF series, the CV curves for the OP samples (Fig. 3c) display distinct redox peaks, confirming a dominant battery-type charge storage behavior. Among these, the OP-800 electrode exhibited the largest CV area, yielding a specific capacitance of 197.7 F/g at 5 mV/s, which significantly outperforms both OP-400 (128.6 F/g) and OP-600 (105.9 F/g). This trend is further validated by the GCD profiles (Fig. 3d), which show non-linear Faradaic plateaus consistent with pseudocapacitance. Consequently, OP-800 achieved the highest specific capacitance of 135.4 F/g at 1 A/g. This enhanced electrochemical performance is ascribed to the superior porosity developed at 800 °C, which effectively increases the abundance of accessible active sites and optimizes ion-diffusion pathways.

3.2. *Development and optimization of green-activated carbon (CFOP)*

Predicated on preliminary studies identifying orange peel (OP) as a potent natural activating agent, a green, in-situ activation strategy was developed to synthesize a composite carbon material. The primary objective was to exploit the synergistic interactions between coffee grounds (CF) and orange peel during co-pyrolysis to engineer a hierarchical carbon architecture with enhanced electrochemical performance. To validate this synthesis protocol, the efficacy of a one-step co-pyrolysis strategy (yielding CFOP at 800 °C) was rigorously compared against a conventional two-step sequence involving the pre-carbonization of CF followed by OP activation (designated as 600ACCOP).

Electrochemical evaluation (Fig. 4) definitively demonstrated the superiority of the one-step strategy. The CFOP electrode displayed a substantially expanded CV curve area (Fig. 4a) a prolonged discharge duration in GCD tests (Fig. 4b), yielding a remarkable specific capacitance of 275.3 F/g at 1 A/g—approximately double that of the 600ACCOP sample (138.4 F/g). Electrochemical Impedance Spectroscopy (EIS) analysis (Fig. 4c) indicated that while both samples possess low equivalent series resistances (R_s of 0.92 Ω for CFOP and 0.76 Ω for 600ACCOP), confirming high intrinsic conductivity, the CFOP electrode exhibited a markedly reduced charge-transfer resistance (R_{ct}) [57–59].

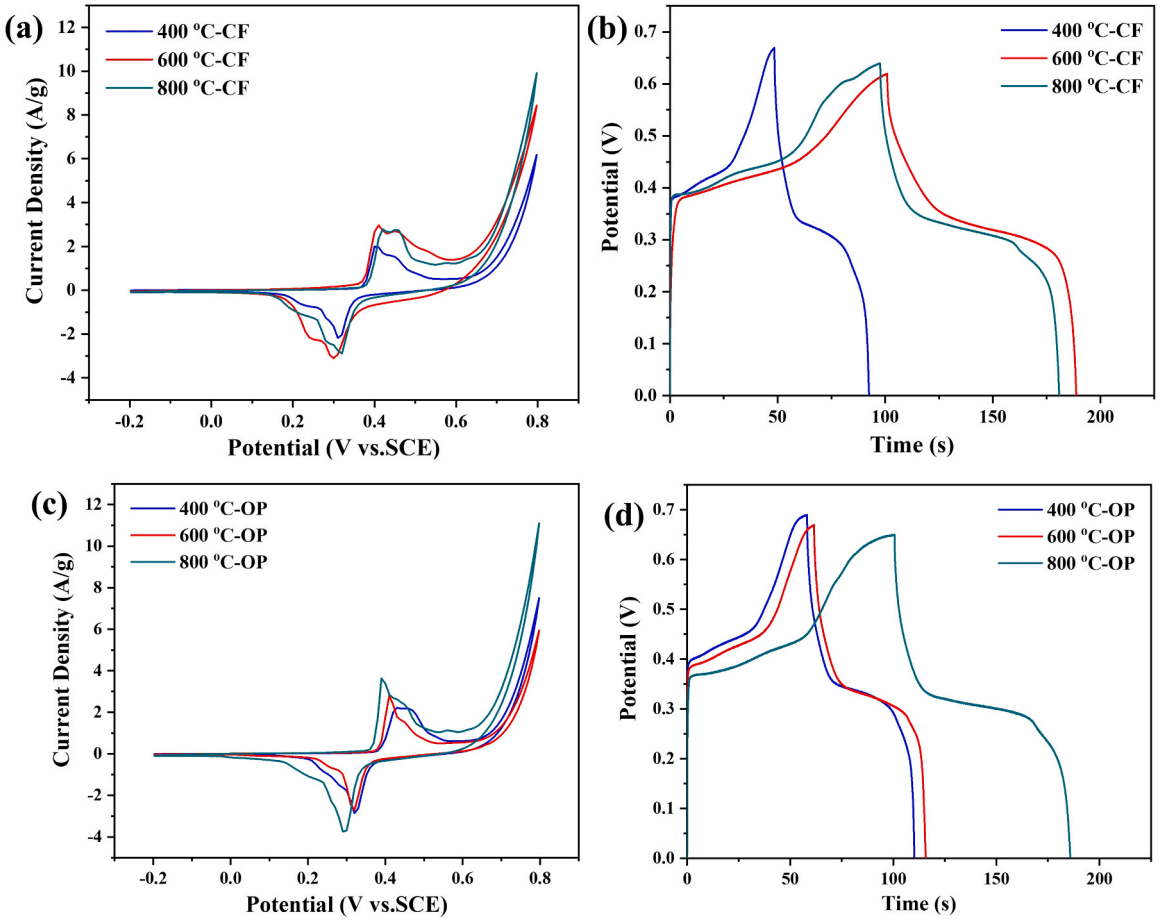


Fig. 3. Electrochemical performance of CF samples carbonized at different temperatures with 3 M KOH as the electrolyte: (a) CV curves at a scan rate of 5 mV/s from −0.2 V to 0.8 V and (b) GCD curves at a current density of 1 A/g. Electrochemical performance of OP samples carbonized at different temperatures with 3 M KOH as the electrolyte: (c) CV curves at a scan rate of 5 mV/s from −0.2 V to 0.8 V and (d) GCD curves at a current density of 1 A/g.

This diminished R_{ct} indicates significantly more facile Faradaic reaction kinetics at the electrode-electrolyte interface. This outcome underscores the vital role of synergistic interfacial interactions occurring during the simultaneous thermal decomposition of the biomass precursors, facilitating the formation of a highly integrated, electrochemically active carbon network that is unattainable via sequential processing.

Upon establishing the one-step co-carbonization process as the optimal synthesis pathway, the critical influence of activation temperature on the material's properties was systematically investigated. As illustrated in Fig. 5, elevating the pyrolysis temperature from 400 °C to 800 °C resulted in a monotonic enhancement in electrochemical performance. Notably, the sample synthesized at 800 °C demonstrated superior electrochemical behavior, exhibiting the most substantial integrated CV curve area (Fig. 5a), the most prolonged GCD plateau (Fig. 5b), and a peak specific capacitance of 275.3 F/g at a current density of 1 A/g. EIS further elucidated the kinetic benefits of high-temperature treatment (Fig. 5c). While the R_s varied-measuring 1.11 Ω, 1.27 Ω, and 0.90 Ω for 400 °C, 600 °C, and 800 °C respectively-the 800 °C sample distinctly achieved the lowest resistance. Moreover, the R_{ct} was minimized at 800 °C, indicating optimized charge-transfer kinetics and highly facile Faradaic reactions at the electrode-electrolyte interface. This significant performance boost is ascribed to the more complete pyrolysis and effective in-situ activation at elevated temperatures, which yields a highly developed porous architecture alongside an enhanced degree of graphitization.

Following the determination of the optimal pyrolysis temperature, the synthesis protocol was further fine-tuned by systematically evaluating both the precursor mass ratio and the coffee roast level. The investigation initially focused on the mass ratio of CF to OP at 800 °C. Electrochemical characterization, as depicted in Fig. 6a and 6b, conclusively identified the 1:1 mass ratio as the optimal composition. This specific ratio exhibited the most extensive CV area (Fig. 6a), the most prolonged GCD profile (Fig. 6b), yielding a peak specific capacitance of 275.3 F/g at 1 A/g, significantly outperforming both the 2:1 and 1:2 ratios. The enhanced electrochemical behavior of the 1:1 ratio is ascribed to an optimal balance of activating species during pyrolysis. Conversely, a 2:1 CF: OP ratio likely provides insufficient activating agents for adequate pore generation, whereas a 1:2 ratio tends to induce excessive etching, resulting in the collapse and structural degradation of the carbon framework.

Subsequently, the impact of the coffee roast level on the electrochemical properties was rigorously evaluated. As illustrated in Fig. 6c and 6d, the electrode derived from light-roast coffee grounds (designated as CFOP(L)) exhibited significantly superior electrochemical performance relative to its dark-roast counterpart (CFOP(D)). Specifically, the CFOP(L) electrode displayed a substantially expanded CV area (Fig. 6c) and a more prolonged GCD plateau (Fig. 6d), achieving a specific capacitance of 275.3 F/g at 1 A/g. This value is more than threefold higher than the 80.8 F/g observed for CFOP(D). This distinct performance disparity is attributed to intrinsic compositional variations: light-roast beans preserve a higher concentration of volatile organic compounds, such as hemicellulose and lipids. These components actively promote pore formation during activation, facilitating the development of a hierarchical porous network [60]. Based on these optimization studies, the ideal synthesis parameters were established as the one-step co-pyrolysis of light-roast coffee grounds and orange peel at

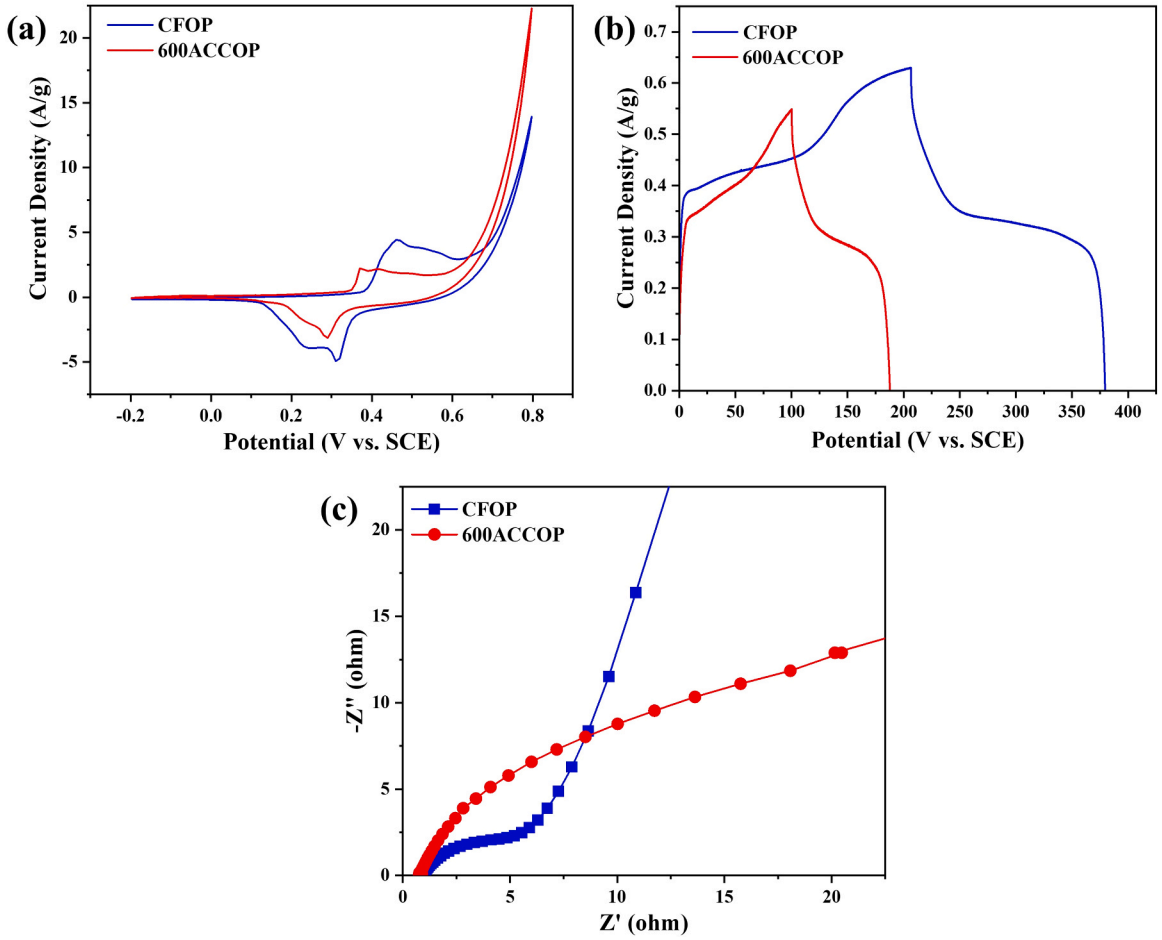


Fig. 4. Electrochemical performance of carbon materials derived from coffee grounds and orange peels prepared via different synthesis routes with 3 M KOH as the electrolyte: (a) CV curves at a scan rate of 5 mV/s from −0.2 V to 0.8 V; (b) GCD curves at a current density of 1 A/g; (c) Nyquist plots.

a 1:1 mass ratio at 800 °C. The optimized composite, denoted hereafter as CFOP, was consequently selected for the detailed structural and electrochemical characterizations presented in the following sections.

3.3. Characterization of the optimized CFOP materials

To elucidate the structural origins of the significantly enhanced electrochemical performance of an orange peel-activated carbon composite (CFOP), a detailed characterization was conducted against its unactivated counterpart (CF), prepared under their respective optimal conditions (CFOP: 1:1 mass ratio at 800 °C; CF: at 600 °C). FESEM revealed that the activation process induced a more developed porous microstructure in CFOP (Fig. 7a). Brunauer-Emmett-Teller (BET) analysis (Figure S4a) revealed that both materials displayed a characteristic type IV isotherm with a hysteresis loop, confirming the presence of mesopores. A significant increase in the specific surface area was observed following activation, rising from 78.5 m^2g^{-1} (CF) to 116.4 m^2g^{-1} (CFOP). The pore size distribution (Figure S4b) confirmed a hierarchical porous architecture (micropores, mesopores, and macropores), with the average pore diameter decreasing from 19.8 nm (CF) to 13.5 nm (CFOP) upon activation [61]. Complementing the surface morphology analysis, X-ray diffraction (XRD) was conducted to provide deeper structural insights (Fig. 7b). Both samples exhibited broad diffraction features characteristic of amorphous carbon, with peaks centered at $2\theta \approx 23.9°$, 43.0°, and 62.0°, which correspond to the (201), (304), and (227) planes of hexagonal carbon (JCPDS No. 20-0258), along with a weaker peak at 29.5°. Crucially, the CFOP sample displayed a distinct intensification of the diffraction peaks at $2\theta \approx 23.9°$ and 29.5°, indicating a higher degree of structural ordering and the development of graphitic domains. Collectively, these results conclusively demonstrate that orange peel acts as an effective in-situ activating agent, yielding synergistic improvements by simultaneously enhancing the material's specific surface area and crystalline order. These combined physical and structural merits ensure abundant active sites, facilitating more efficient charge transport and directly accounting for the superior electrochemical performance of the CFOP materials.

To comprehensively investigate the microstructure and elemental composition of the optimized CFOP materials, field-emission transmission electron microscopy (FETEM) was employed, as depicted in Fig. 8. The low-magnification FETEM image (Fig. 8a) reveals a uniform and interconnected morphology that corroborates the FESEM observations, indicating the formation of a robust, well-organized carbon framework. As shown in Fig. 8b, the selected-area electron diffraction (SAED) pattern displays well-defined concentric rings, confirming the material's polycrystalline nature. These rings are indexed to the (201), (203), (304), and (227) planes of the hexagonal carbon phase (JCPDS No. 20–0258), which aligns with the crystallographic features identified in the XRD analysis. For further detail, the indexed diffraction rings, corresponding d-spacing values, and crystal plane assignments are summarized in Table S1. High-resolution TEM (HRTEM) analysis (Fig. 8c) further unveils well-defined lattice fringes embedded within an amorphous matrix. The measured interplanar spacings of 0.303 nm, 0.210 nm, and 0.150 nm correspond to the (201), (203), and (304) planes of the hexagonal carbon phase, providing direct nanoscale evidence of the crystalline domains formed during activation. The elemental composition and spatial distribution were assessed via

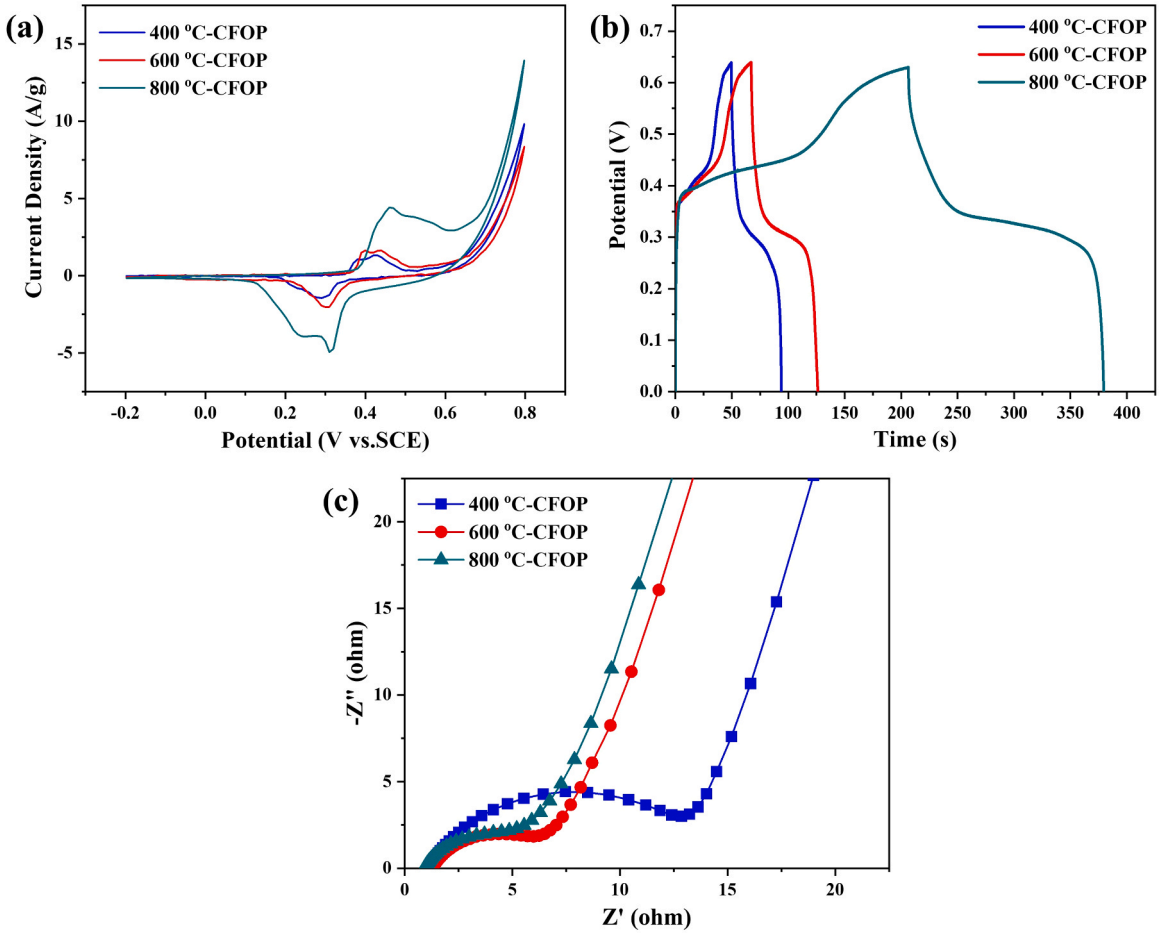


Fig. 5. Electrochemical performance of CFOP samples prepared at different activation temperatures with 3 M KOH as the electrolyte: (a) CV curves at a scan rate of 5 mV/s from −0.2 V to 0.8 V; (b) GCD curves at a current density of 1 A/g; (c) Nyquist plots.

energy-dispersive X-ray spectroscopy (EDS). The elemental mapping (Fig. 8d) confirms a homogeneous distribution of carbon (C), oxygen (O), and potassium (K) throughout the matrix. The corresponding EDS spectrum (Fig. 8e) also detects nitrogen (N), originating from the intrinsic nitrogen-containing organic compounds in the biomass precursors. Quantitative analysis determines the average atomic composition of the CFOP materials to be C (66.4 at%), O (29.7 at%), N (2.8 at%), and K (1.1 at%). Notably, the presence of potassium—primarily derived from the coffee grounds—is of particular significance. Residual potassium acts as an in-situ activating agent during pyrolysis, catalyzing carbon etching and facilitating the development of porous structures. Consequently, the retention of trace K in the final product likely contributes to the hierarchical porosity observed in CFOP, thereby enhancing electrolyte accessibility and boosting electrochemical performance [62].

X-ray photoelectron spectroscopy (XPS) was used to determine the elemental composition and chemical bonding states of the optimized CFOP materials. The survey spectrum (Fig. 9a) confirmed the incorporation of C, K, N, and O within the composite. High-resolution spectra were subjected to Gaussian curve fitting to elucidate specific chemical configurations (Fig. 9b-d). The C 1 s spectrum (Fig. 9b) resolved into two primary components at 284.7 eV and 289.4 eV, corresponding to C═C sp^2 bonds and C═O groups, respectively [63]. Simultaneously, the K 2p spectrum showed characteristic spin-orbit doublets, K $2p_{3/2}$ and K $2p_{1/2}$, at 292.9 eV and 295.5 eV, respectively [64,65]. Analysis of the N 1 s spectrum (Fig. 9c) revealed the presence of pyridinic N (399.8 eV) and pyrrolic N (404.1 eV), functionalities that enhance electrochemical performance by acting as catalytically active sites [66,67]. The O 1 s spectrum (Fig. 9d) was fitted to three distinct states: C═O (529.8 eV), O–H or C–O–C (531.3 eV), and O–C═O (533.0 eV) [68–70]. This detailed XPS characterization conclusively validates the successful synthesis of the CFOP materials, reinforcing the compositional and structural findings established from prior XRD and EDS analyses.

3.4. Electrochemical evaluation of the optimized CFOP materials

A comprehensive electrochemical evaluation was conducted to determine the charge storage performance of the optimized CFOP electrode, as summarized in Fig. 10. The rate capability was initially assessed via CV across a range of scan rates, depicted in Fig. 10a. As the scan rate increased, the anodic and cathodic peaks displayed a progressive shift toward more positive and negative potentials, respectively. This behavior is intrinsic to battery-type electrodes and is predominantly ascribed to enhanced electrode polarization at elevated scan rates [71]. Despite this anticipated peak shift, the CV profiles maintained well-defined shapes with negligible distortion even at the highest scan rate. This stability indicates that the CFOP electrode possesses low internal resistance, facilitating efficient ion diffusion and charge transport throughout the porous carbon framework [72]. Quantitative analysis revealed that the specific capacitances, derived from the CV curves at 5, 10, 20, 50, 80, and 100 mV/s, were 376.9, 340.9, 286.3, 187.2, 148.7, and 131.5 F/g, respectively. These results substantiate the material's excellent rate capability.

The GCD profiles recorded at various current densities are depicted in Fig. 10b. The highly symmetrical nature of the charge and discharge curves signifies the excellent electrochemical reversibility and high

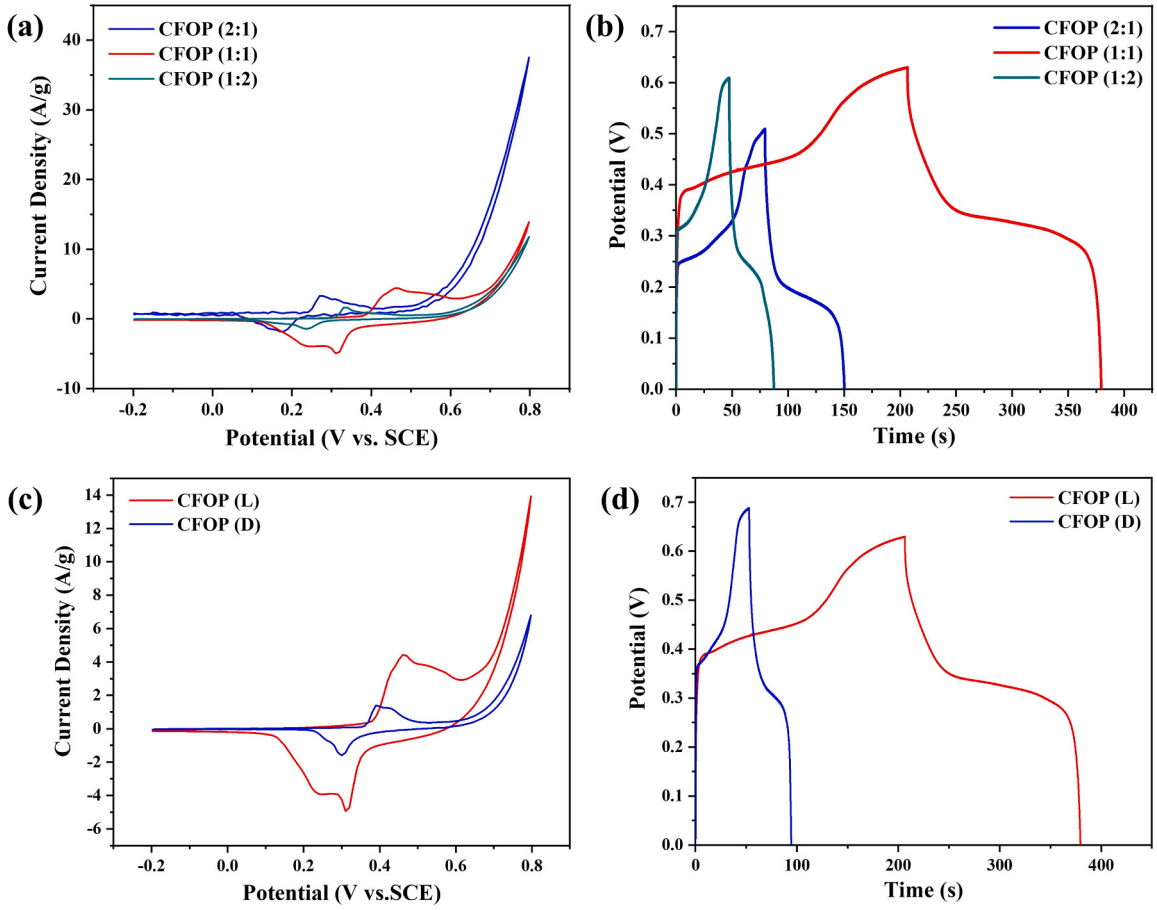


Fig. 6. Electrochemical performance of CFOP samples prepared with different coffee ground to orange peel mass ratios with 3 M KOH as the electrolyte: (a) CV curves at a scan rate of 5 mV/s from −0.2 V to 0.8 V and (b) GCD curves at a current density of 1 A/g. Electrochemical performance of CFOP samples derived from coffee grounds with different roast levels with 3 M KOH as the electrolyte: (c) CV curves at a scan rate of 5 mV/s from −0.2 V to 0.8 V and (d) GCD curves at a current density of 1 A/g.

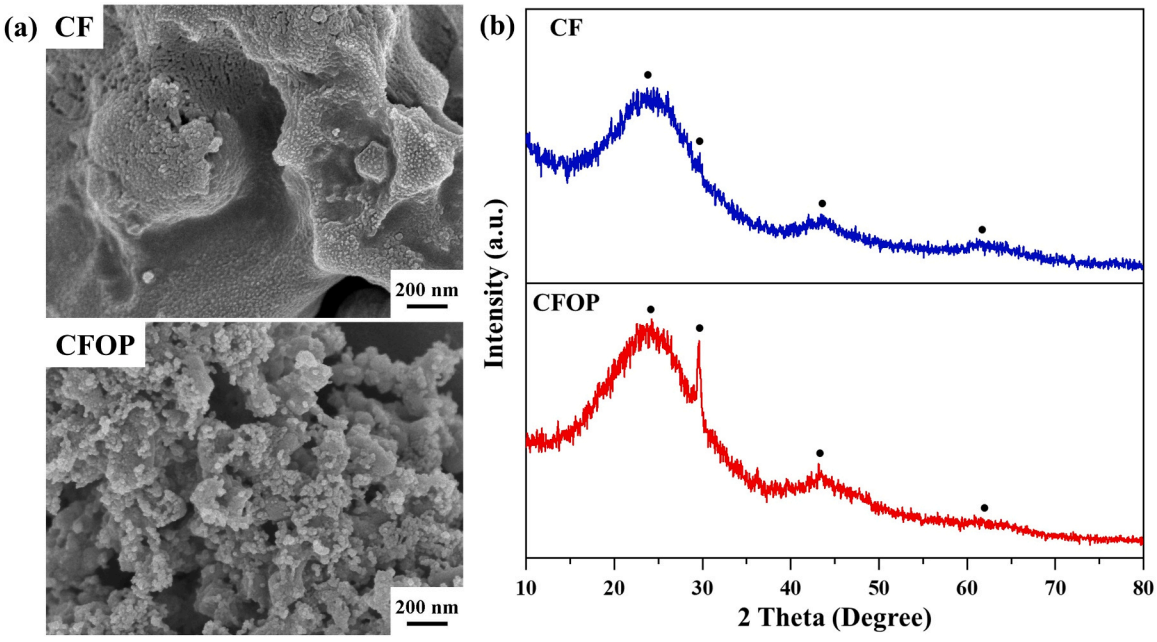


Fig. 7. The (a) FESEM images and (b) XRD patterns of pre-activated (CF) and activated (CFOP) materials.

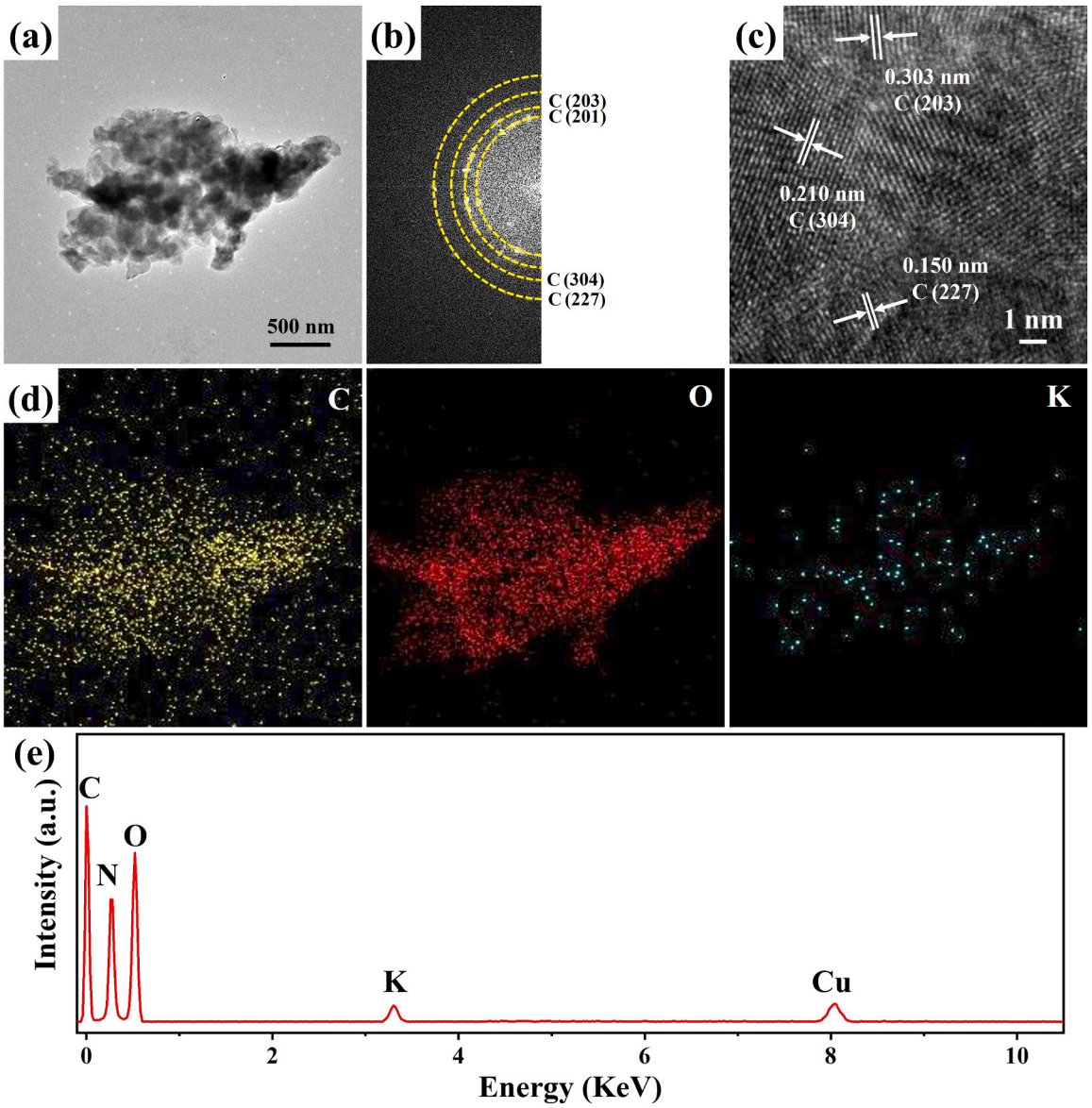


Fig. 8. (a) FETEM images, (b) SAED pattern, (c) HRTEM image, (d) EDS mapping images, and (e) EDS spectrum of CFOP materials.

coulombic efficiency of the CFOP electrode [72]. As summarized in Fig. 10c, an increase in current density corresponds to a progressive reduction in specific capacitance. This behavior is characteristic of battery-type materials and is principally ascribed to two factors: (i) the comparatively sluggish kinetics of the Faradaic ion intercalation/deintercalation processes, and (ii) the elevated diffusion resistance of electrolyte ions at higher rates, which restricts the full utilization of the active material volume [73]. Specifically, the calculated specific capacitances at current densities of 1, 2, 5, 8, and 10 A/g were 275.3, 111.5, 29.5, 12.9, and 8.1 F/g, respectively, underscoring the rate-dependent characteristics of the charge storage mechanism. To contextualize these results, Table S2 provides a comparative overview of reported supercapacitor electrode materials. While the majority of cited studies rely on conventional chemical activation methods, the CFOP materials developed in this work distinguishes itself by utilizing orange peel (OP) as a natural activating agent. Unlike harsh chemical activation, the OP-based approach is significantly more environmentally benign and mitigates the risk of severe structural degradation or corrosion of the carbon framework. Moreover, the CFOP materials exhibit specific capacitance values superior to most comparable samples listed. This confirms that our synthesis strategy not only achieves exceptional electrochemical performance but also successfully synergizes environmental sustainability with economic viability.

Fig. 10d illustrates the coulombic efficiency of the CFOP electrode as a function of current density. The recorded efficiencies were 92.6 %, 95.0 %, 98.1 %, 97.8 %, and 98.5 % at current densities of 1, 2, 5, 8, and 10 A/g, respectively. The relatively suppressed efficiency observed at 1 A/g is primarily ascribed to the incipient formation of a solid-electrolyte interphase (SEI) on the electrode surface. This phenomenon entails irreversible parasitic reactions that consume charge during the initial cycling stages, consequently lowering the initial efficiency. However, the establishment of a robust SEI layer is ultimately beneficial; it effectively passivates the electrode surface and inhibits further electrolyte decomposition, thereby augmenting long-term cycling stability and extending electrode lifespan [74]. The consistently high coulombic efficiencies achieved at elevated current densities attest to the superior electrochemical reversibility and structural stability of the CFOP electrode under dynamic operating conditions.

To further elucidate the charge-storage mechanism of the optimized CFOP electrode, a detailed kinetic analysis was performed using CV data obtained at various scan rates. The purpose of this analysis is to determine whether the electrochemical behavior is primarily governed by

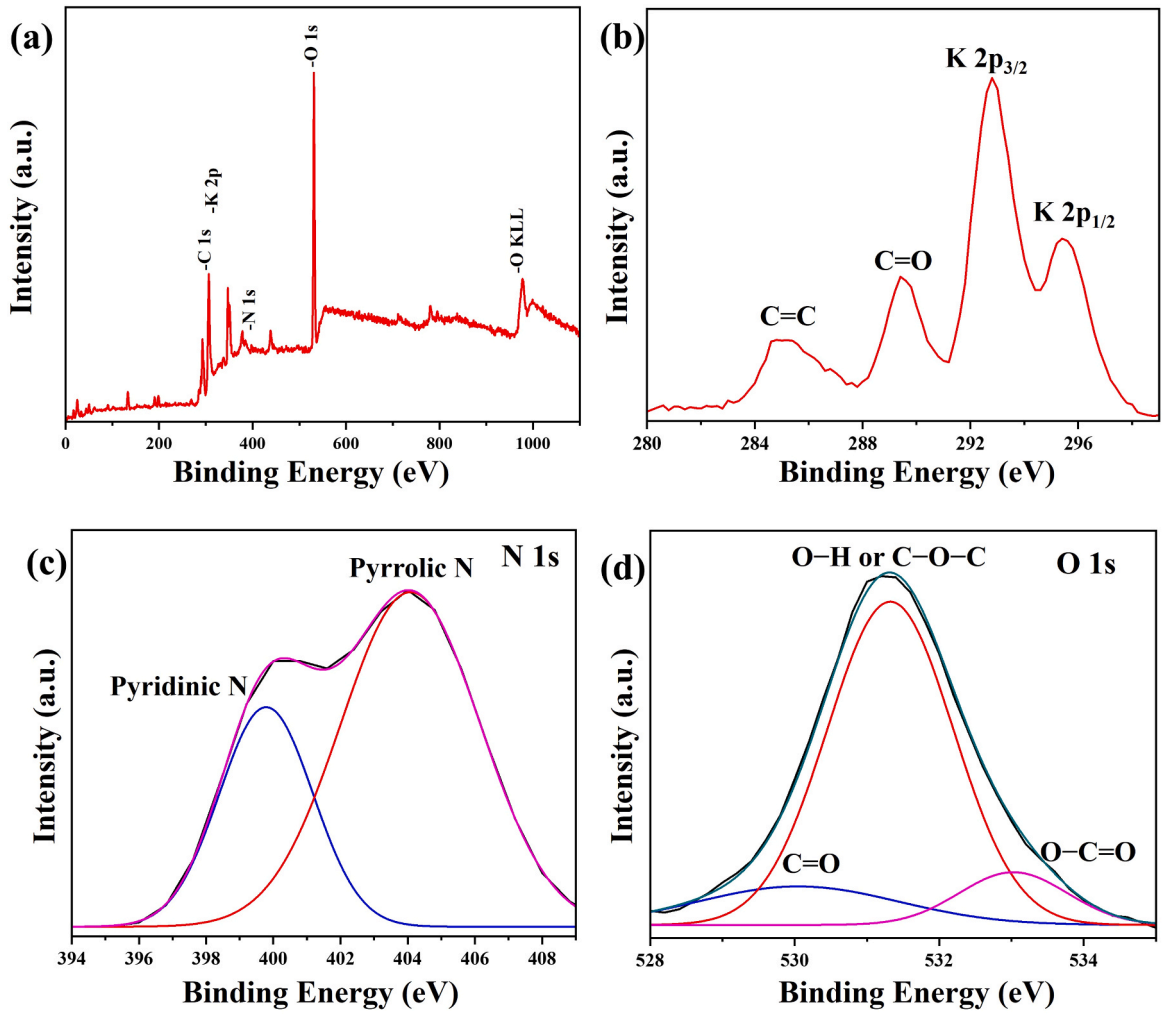


Fig. 9. (a) XPS survey spectrum of the optimized CFOP materials. The high-resolution XPS spectra of (b) C 1 s and K 2p, (c) N 1 s, and (d) O 1 s in the optimized CFOP materials.

diffusion-controlled Faradaic reactions or by surface-controlled capacitive processes, thereby providing a deeper understanding of the factors influencing the electrode's performance [75]. Initially, the relationship between the peak current (i) and the square root of the scan rate ($\nu^{1/2}$) was examined. As shown in Fig. 11a, the anodic and cathodic peak currents exhibit strong linearity with $\nu^{1/2}$ ($R^2 = 0.999$), confirming that diffusion-controlled kinetics play a dominant role in the reaction process. To more precisely quantify the kinetic contributions, the dependence of peak current on scan rate was further analyzed using the power-law relationship shown in Eq. (1), converted into its logarithmic form in Eq. (2).

$$i = a\nu^b \tag{1}$$

$$\log(i) = \log(a) + b\log(\nu) \tag{2}$$

where i is the peak current, ν is the scan rate, and a and b are adjustable constants. The b-value, determined from the slope of the log (i) vs. log(ν) plot, is indicative of the charge storage mechanism. A b-value of 0.5 signifies a purely diffusion-controlled process (battery-like), while a b-value of 1.0 indicates a surface-controlled capacitive process. A value between 0.5 and 1.0 suggests a hybrid mechanism involving both processes [76–78]. Fig. 11b displays the linear fit of log(i) versus log(ν). From the slopes, the b-values for the anodic and cathodic peaks were calculated to be 0.59 and 0.54, respectively. As both values are close to 0.5, this confirms that the energy storage in the CFOP electrode is predominantly diffusion-controlled, with a minor contribution from surface capacitance. To quantitatively separate the diffusion-controlled and capacitive contributions, the current response (i) at a specific potential (V) was further analyzed using Eq. (3), which can be rearranged to the linear form in Eq. (4) [76–78]:

$$i(V) = k_1\nu + k_2\nu^{1/2} \tag{3}$$

$$i(V)/\nu^{1/2} = k_1\nu^{1/2} + k_2 \tag{4}$$

Where $k_1\nu$ represents the current from surface-capacitive effects and $k_2\nu^{1/2}$ represents the current from diffusion-controlled intercalation processes. By obtaining the values of k_1 and k_2 from the plot of $i/\nu^{1/2}$ vs. $\nu^{1/2}$, the fractional contribution of each process can be calculated. The calculated contribution ratios at various scan rates are depicted in Fig. 11c and 11d. At a low scan rate of 5 mV/s, the diffusion-controlled process accounts for 95 % of the total charge storage. As the scan rate increases, the diffusion-controlled contribution systematically decreases, reaching 80 % at 100 mV/s. Correspondingly, the surface-capacitive contribution increases from 5 % to 20 %. This trend is attributed to the fact that at higher scan rates, electrolyte ions have insufficient time to diffuse into the bulk of the electrode material to undergo Faradaic reactions. Consequently, the faster, non-diffusion-limited surface capacitive processes become more prominent [77].

To assess the long-term durability and practical applicability of the optimized CFOP materials, its cycling stability and coulombic efficiency were evaluated over 5000 consecutive galvanostatic charge–discharge (GCD) cycles at a current density of 1 A/g. The corresponding

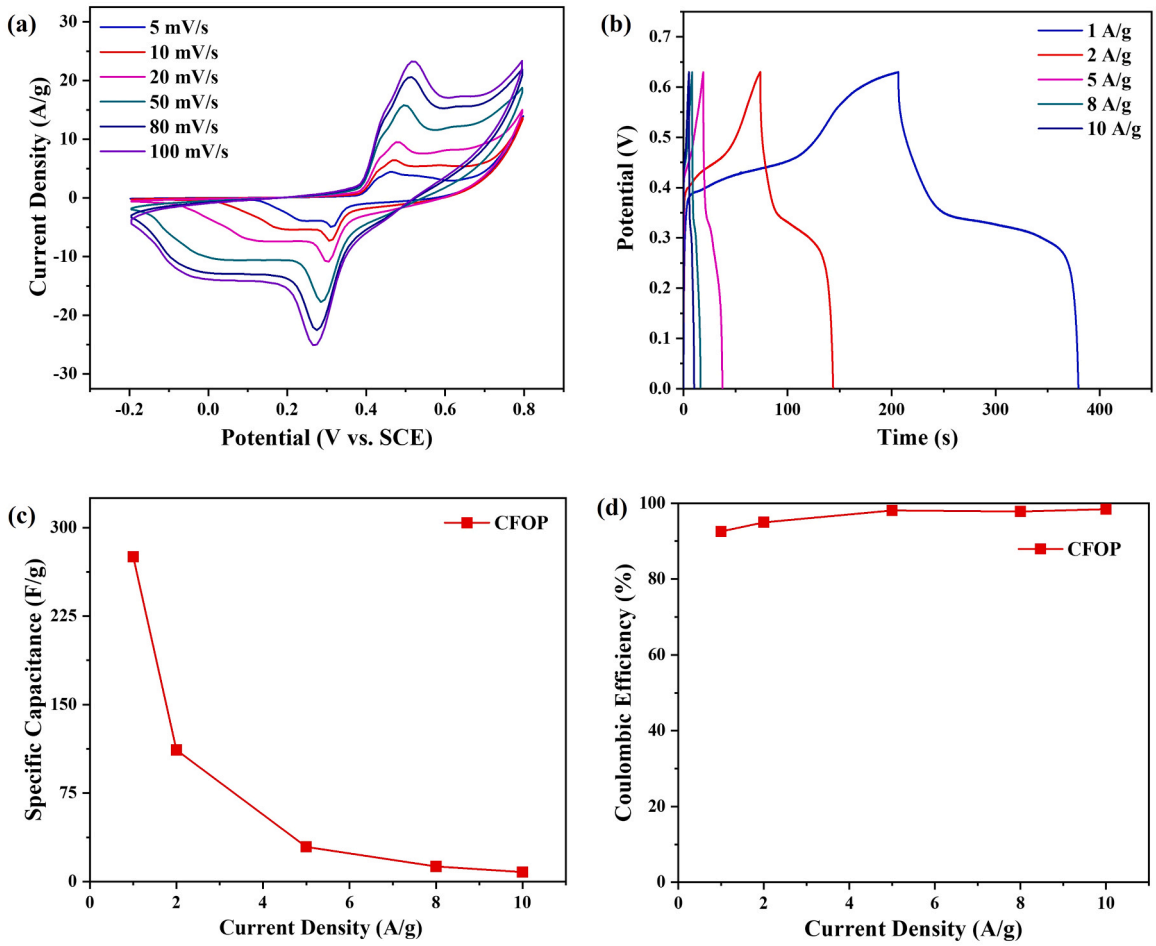


Fig. 10. Electrochemical characterization of the optimized CFOP electrode with 3 M KOH as the electrolyte: (a) CV curves at various scan rates from −0.2 V to 0.8 V; (b) GCD curves at different current densities; (c) Comparison of specific capacitance values at varying current densities; (d) Coulombic efficiency as a function of current density.

performance data are presented in Fig. 12. As shown, the CFOP electrode exhibits a gradual decrease in specific capacitance over prolonged cycling, a typical behavior for diffusion-dominated pseudocapacitive materials. This decline is primarily due to mechanical stress and structural degradation caused by repeated ion insertion and extraction during redox reactions. Specifically, the main degradation mechanism is identified as the mechanical failure and detachment of the active material from the current collector. Observation of the post-cycling FESEM image (Figure S5) reveals noticeable areas where the CFOP active material has peeled off from the nickel foam substrate, confirming that the loss of physical contact and subsequent detachment of the electrode material is a major contributors to the capacitance decay and reduced cyclic performance. Interestingly, a notable increase in capacitance is observed during the initial ~200 cycles, with retention exceeding 100 %. This phenomenon is commonly ascribed to an electrochemical activation process, wherein progressive electrolyte infiltration into the porous structure enhances the accessibility of electroactive sites that were initially unavailable. Moreover, a slight recovery in capacitance retention is evident toward the end of the cycling test, potentially due to partial exfoliation of the electrode surface. This mechanical alteration may expose fresh active interfaces, thereby facilitating renewed electrochemical activity. After 5000 cycles, the CFOP electrode retains 63.27 % of its initial specific capacitance, demonstrating commendable structural resilience. Additionally, the coulombic efficiency remains consistently high throughout the test, with a final value of 97.29 %, indicating excellent electrochemical reversibility. These results collectively confirm that CFOP possesses promising long-term cycling stability and is a viable candidate for practical energy storage applications.

4. Conclusions

In conclusion, this study successfully established a highly effective, green, and scalable one-step co-pyrolysis strategy for synthesizing hierarchical porous carbon (CFOP) from two abundant biowaste streams: waste coffee grounds (precursor) and orange peels (natural activator). The synergistic in-situ activation, driven by both the residual potassium from the coffee grounds and the volatile organic compounds from the orange peels, was critical in engineering the resulting superior electrode material. The optimized CFOP, prepared at 800 °C with a 1:1 mass ratio of light-roast components, demonstrated exceptional electrochemical performance in a three-electrode configuration, achieving a high specific capacitance of 275.3 F/g at 1 A/g. In addition, the electrode showed remarkable long-term stability, retaining 63.27 % of its original capacitance after 5000 charge–discharge cycles, with a consistently high coulombic efficiency of 97.29 %. Structural analysis confirmed enhanced graphitization, while kinetic analysis explicitly verified a diffusion-dominated pseudocapacitive storage mechanism. This finding is significant as it confirms the material's potential beyond traditional double-layer capacitance and establishes it as a viable pseudocapacitive/hybrid material. The primary significance of this work lies in providing a genuine waste-to-wealth pathway, offering a highly efficient and environmentally benign method to convert high-volume food waste into a high-value functional material for energy storage. For industrial commercialization, future research must focus on quantitative

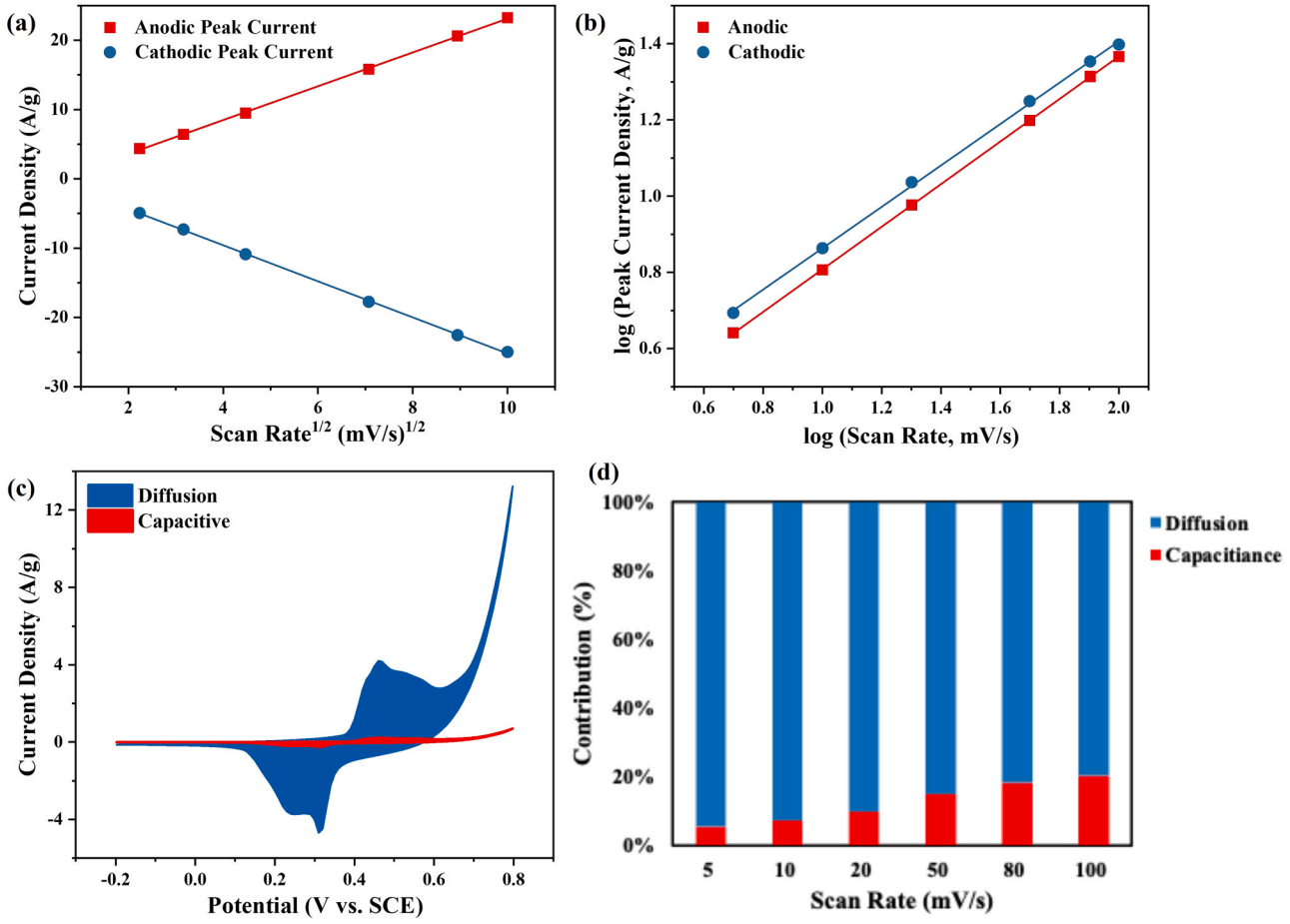


Fig. 11. Kinetic analysis of the optimized CFOP electrode with 3 M KOH as the electrolyte: (a) Linear dependence of anodic/cathodic peak current density on the square root of the scan rate; (b) Log–log plot of anodic/cathodic peak current versus scan rate; (c) Contribution of capacitive and diffusion-controlled processes at a scan rate of 5 mV/s; (d) Proportional contributions of capacitive and diffusion-controlled charge storage at various scan rates.

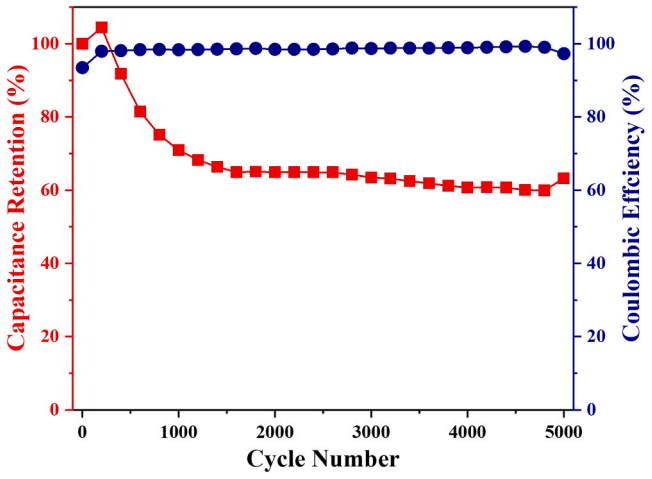


Fig. 12. Cycling stability and coulombic efficiency of the optimized CFOP electrode over 5000 charge–discharge cycles at a current density of 1 A/g with 3 M KOH as the electrolyte.

optimization of production yield and a complete techno-economic analysis to address challenges related to feedstock variability and continuous process control for large-scale manufacturing.

CRediT authorship contribution statement

Yu-Cheng Chang: Writing – review & editing, Writing – original draft, Visualization, Supervision, Software, Resources, Project administration, Methodology, Funding acquisition, Conceptualization. **Shao-Ru Chang:** Validation, Investigation, Formal analysis, Data curation.

Declaration of Competing Interest

The authors declare the following financial interests/personal relationships which may be considered as potential competing interests: Yu-Cheng Chang reports financial support was provided by National Science and Technology Council. If there are other authors, they declare that they have no known competing financial interests or personal relationships that could have appeared to influence the work reported in this paper.

Acknowledgments

The authors sincerely thank the National Science and Technology Council (NSTC) of Taiwan for the financial support provided under project numbers NSTC-112-2221-E-035-017-MY3 and NSTC-113-2221-E-035-023-MY3. This support played a vital role in enabling the successful completion of this research.

Appendix A. Supporting information

Supplementary data associated with this article can be found in the

online version at doi:10.1016/j.jece.2025.120742.

Data availability

No data was used for the research described in the article.

References

[1] N. Armaroli, V. Balzani, The legacy of fossil fuels, Chem. Asian J. 6 (2011) 768–784.
[2] Afifa, K. Arshad, N. Hussain, M.H. Ashraf, M.Z. Saleem, Air pollution and climate change as grand challenges to sustainability, Sci. Total Environ. 928 (2024) 172370.
[3] M. Shahbaz, A. Siddiqui, M. Siddiqui, Z. Jiao, P. Kautish, Exploring the growth of sustainable energy technologies: a review, Sustain Energy Technol. Assess. 57 (2023) 103157.
[4] S. Su, M. Qamruzzaman, S. Karim, Charting a sustainable future: the impact of economic policy, environmental taxation, innovation, and natural resources on clean energy consumption, Sustainability (2023).
[5] A.G. Olabi, K. Elsaid, K. Obaideen, M.A. Abdelkareem, H. Rezk, T. Wilberforce, et al., Renewable energy systems: Comparisons, challenges and barriers, sustainability indicators, and the contribution to UN sustainable development goals, Int. J. Thermofluids 20 (2023) 100498.
[6] A.A. Bazmi, G. Zahedi, Sustainable energy systems: role of optimization modeling techniques in power generation and supply—a review, Renew. Sust. Energy Rev. 15 (2011) 3480–3500.
[7] M. Yekini Suberu, M. Wazir Mustafa, N. Bashir, Energy storage systems for renewable energy power sector integration and mitigation of intermittency, Renew. Sust. Energy Rev. 35 (2014) 499–514.
[8] E.T. Sayed, A.G. Olabi, A.H. Alami, A. Radwan, A. Mdallal, A. Rezk, et al., Renewable energy and energy storage systems, Energies 16 (2023) 1415.
[9] K. Madhumitha, A.S. Nesaraj, M.K. Paramathma, Advancements in high-performance perovskite nanostructured electrodes for next-generation electrochemical supercapacitors: a comprehensive review, Inorg. Chem. Commun. 182 (2025) 115379.
[10] R.T. Yadlapalli, R.R. Alla, R. Kandipati, A. Kotapati, Super capacitors for energy storage: progress, applications and challenges, J. Energy Storage 49 (2022) 104194.
[11] J. Yan, Q. Wang, T. Wei, Z. Fan, Recent advances in design and fabrication of electrochemical supercapacitors with high energy densities, Adv. Energy Mater. 4 (2014) 1300816.
[12] X. Shen, H. Liu, X.-B. Cheng, C. Yan, J.-Q. Huang, Beyond lithium ion batteries: higher energy density battery systems based on lithium metal anodes, Energy Storage Mater. 12 (2018) 161–175.
[13] W. Cao, J. Zhang, H. Li, Batteries with high theoretical energy densities, Energy Storage Mater. 26 (2020) 46–55.
[14] X. Zhao, B.M. Sánchez, P.J. Dobson, P.S. Grant, The role of nanomaterials in redox-based supercapacitors for next generation energy storage devices, Nanoscale 3 (2011) 839–855.
[15] Z. Wu, L. Li, J.-m Yan, X.-b Zhang, Materials design and system construction for conventional and new-concept supercapacitors, Adv. Sci. 4 (2017) 1600382.
[16] A.G. Olabi, Q. Abbas, A. Al Makky, M.A. Abdelkareem, Supercapacitors as next generation energy storage devices: properties and applications, Energy 248 (2022) 123617.
[17] A. Afif, S.M.H. Rahman, A. Tasfiah Azad, J. Zaini, M.A. Islan, A.K. Azad, Advanced materials and technologies for hybrid supercapacitors for energy storage – a review, J. Energy Storage 25 (2019) 100852.
[18] S. Singh, M.B. Gumpu, Sheeba K.N., S.K. Paramasivam, A comprehensive evaluation of synthesis methods for porous carbon materials and their applications in energy storage, Diam. Relat. Mater. 153 (2025) 112033.
[19] L. Guan, D. Li, S. Ji, X. Wei, F. Meng, Structural regulation and performance enhancement of carbon-based supercapacitors: insights into electrode material engineering, Materials (2025).
[20] W. Tian, H. Zhang, X. Duan, H. Sun, G. Shao, S. Wang, Porous carbons: structure-oriented design and versatile applications, Adv. Funct. Mater. 30 (2020) 1909265.
[21] Q. Tang, X. Chen, D. Zhou, C. Liu, Biomass-derived hierarchical porous carbon/silicon carbide composite for electrochemical supercapacitor, Colloids Surf. A Physicochem. Eng. Asp. 620 (2021) 126567.
[22] L. Qin, Z. Hou, S. Lu, S. Liu, Z. Liu, E. Jiang, Porous carbon derived from pine nut shell prepared by steam activation for supercapacitor electrode material, Int. J. Electrochem. Sci. 14 (2019) 8907–8918.
[23] D. Thomas, N.B. Fernandez, M.D. Mullassery, R. Surya, L.E. Jacob, Banana stem biochar composite with polyaniline for energy storage applications, Results Chem. 6 (2023) 101088.
[24] A. Bamisaye, M.A. Adekola, S.M. Abati, N.O. Etafo, O.S. Ademola, P.T. Joseph, et al., Recent advances in metal/metal-oxide nanoparticle-polymer nanohybrid for biomedical applications, Mater. Today Chem. 49 (2025) 103086.
[25] G. Durán-Jiménez, J. Rodriguez, L. Stevens, E.T. Kostas, C. Dodds, Microwave pyrolysis of waste biomass and synthesis of micro-mesoporous activated carbons: The role of textural properties for CO2 and textile dye adsorption, Chem. Eng. J. 488 (2024) 150926.
[26] A. Güngör, D. Şentürk, D. Eşkin, İ. Aksoy, E.C. Kılınç, E. Erdem, Organic waste-derived activated carbons for supercapacitor applications: advances in synthesis strategies and electrochemical performance enhancement, Phys. Status Solidi (a) (2025) 2400992.
[27] J. Sun, H. Li, Q. Liu, W. Zhong, W. Dong, Recent advances in biomass-derived porous carbons for post-combustion CO2 capture: from preparation and adsorption mechanisms to applications, Chem. Eng. J. 520 (2025) 165890.
[28] V. Filimonau, M. Krivcova, F. Pettit, An exploratory study of managerial approaches to food waste mitigation in coffee shops, Int. J. Hosp. Manag. 76 (2019) 48–57.
[29] T. Li, Y. Wang, S. Qi, J. Su, S. Liu, Y. Bai, et al., Spent coffee grounds enhanced ferrous-driven microbial denitrification: synergistic removal mechanisms for nitrate and acetaminophen, J. Environ. Chem. Eng. 13 (2025) 119701.
[30] M.R. Uddin, M.H. Mustak, M. Nuruzzaman, F. Ahmed, J. Tazrin, M.A. Rahman, et al., Optimized H3PO4 activation of Nypa fruticans roots for high-performance activated carbon: structural control and enhanced iodine adsorption, Biomass Bioenergy 205 (2026) 108488.
[31] R. Campos-Vega, G. Loarca-Piña, H.A. Vergara-Castañeda, B.D. Oomah, Spent coffee grounds: a review on current research and future prospects, Trends Food Sci. Technol. 45 (2015) 24–36.
[32] J. McNutt, Q. He, Spent coffee grounds: a review on current utilization, J. Ind. Eng. Chem. 71 (2019) 78–88.
[33] S.A. Aguilar-Maruri, L. Ramos-Galicia, R. Ocampo-Pérez, A. Forgionny, B. Ruíz-Camacho, J.C. Serna-Carrizales, et al., Waste-derived catalytic hydrochars from coffee grounds doped with BiOCl, CeO2, and α-Fe2O3: structural insights and enhanced photocatalytic performance, J. Environ. Chem. Eng. 13 (2025) 117799.
[34] C. Qin, H. Wang, X. Yuan, T. Xiong, J. Zhang, J. Zhang, Understanding structure-performance correlation of biochar materials in environmental remediation and electrochemical devices, Chem. Eng. J. 382 (2020) 122977.
[35] S. Rawat, C.-T. Wang, C.-H. Lay, S. Hotha, T. Bhaskar, Sustainable biochar for advanced electrochemical/energy storage applications, J. Energy Storage 63 (2023) 107115.
[36] V. Negro, B. Ruggeri, D. Fino, D. Tonini, Life cycle assessment of orange peel waste management, Resour. Conserv. 127 (2017) 148–158.
[37] S.S. Lam, R.K. Liew, Y.M. Wong, P.N.Y. Yek, N.L. Ma, C.L. Lee, et al., Microwave-assisted pyrolysis with chemical activation, an innovative method to convert orange peel into activated carbon with improved properties as dye adsorbent, J. Clean. Prod. 162 (2017) 1376–1387.
[38] A.P. Khedulkar, W.-J. Yu, V.D. Dang, B. Pandit, R.-a Doong, Boosting supercapacitor performance with a cobalt hydroxide in-situ preparation orange peel biochar flower-like composite, J. Energy Storage 81 (2024) 110302.
[39] R.G. Freeman, M.B. Hommer, K.C. Grabar, M.A. Jackson, M.J. Natan, Ag-Clad Au nanoparticles: novel aggregation, optical, and surface-enhanced Raman scattering properties, J. Phys. Chem. 100 (1996) 718–724.
[40] A.P. Khedulkar, B. Pandit, V.D. Dang, R.-a Doong, Agricultural waste to real worth biochar as a sustainable material for supercapacitor, Sci. Total Environ. 869 (2023) 161441.
[41] P. Manasa, S. Sambasivam, F. Ran, Recent progress on biomass waste derived activated carbon electrode materials for supercapacitors applications—a review, J. Energy Storage 54 (2022) 105290.
[42] J.F. Peters, D. Iribarren, J. Dufour, Biomass pyrolysis for biochar or energy applications? A life cycle assessment, Environ. Sci. Technol. 49 (2015) 5195–5202.
[43] D. Lohita, H.P. Kavitha, S. Abinaya, T.V. Rajendran, M. Prakash, Biomass derived carbon-metal oxide composite with rare earth metal: towards high energy symmetric supercapacitor, Inorg. Chem. Commun. 182 (2025) 115604.
[44] L. Leng, Q. Xiong, L. Yang, H. Li, Y. Zhou, W. Zhang, et al., An overview on engineering the surface area and porosity of biochar, Sci. Total Environ. 763 (2021) 144204.
[45] R. Mehdi, A.H. Khoja, S.R. Naqvi, N. Gao, N.A. Amin, A review on production and surface modifications of biochar materials via biomass pyrolysis process for supercapacitor applications, Catalysts 12 (2022) 798.
[46] L. Hou, Z. Hu, X. Wang, L. Qiang, Y. Zhou, L. Lv, et al., Hierarchically porous and heteroatom self-doped graphitic biomass carbon for supercapacitors, J. Colloid Interface Sci. 540 (2019) 88–96.
[47] S.-x Yan, Q. Wang, S.-h Luo, Y.-h Zhang, X. Liu, Y.-g Liu, et al., Coal-based S hybrid self-doped porous carbon for high-performance supercapacitors and potassium-ion batteries, J. Power Sources 461 (2020) 228151.
[48] C.-F. Xue, Y.-Y. Wei, R.-C. Huang, W. Zhao, T. Wu, X.-H. Li, et al., Magnesium oxide scaffolded preparation of N, O self-doped biochar with super-hydrophilic surface for aqueous supercapacitor with desired energy density, J. Energy Storage 53 (2022) 105193.
[49] X. Zhang, C. Chen, C. Tang, Y. Wang, Morphological control of biochar with emerging functionalities by thermodynamic and kinetic approaches, Acc. Mater. Res 3 (2022) 525–539.
[50] M. Gupta, N. Savla, C. Pandit, S. Pandit, P.K. Gupta, M. Pant, et al., Use of biomass-derived biochar in wastewater treatment and power production: a promising solution for a sustainable environment, Sci. Total Environ. 825 (2022) 153892.
[51] L. Xie, F. Su, L. Xie, X. Guo, Z. Wang, Q. Kong, et al., Effect of pore structure and doping species on charge storage mechanisms in porous carbon-based supercapacitors, Mater. Chem. Front. 4 (2020) 2610–2634.
[52] D. Malagón-Romero, A.C. Torres-Velasquez, L.K. Tinoco-Navarro, J.P. Arrubla-Vélez, Pyrolysis of Colombian spent coffee grounds (SCGs), characterization of bio-oil, and study of its antioxidant properties, Int. J. Sustain. Energy 42 (2023) 811–829.
[53] P. Connor, J. Schuch, B. Kaiser, W. Jaegermann, The determination of electrochemical active surface area and specific capacity revisited for the system MnOx as an oxygen evolution catalyst 234 (2020) 979–994.

[54] A. Fagan-Murphy, S. Kataria, B.A. Patel, Electrochemical performance of multi-walled carbon nanotube composite electrodes is enhanced with larger diameters and reduced specific surface area, J. Solid State Electrochem. 20 (2016) 785–792.
[55] S. Urbonaite, L. Hälldahl, G. Svensson, Raman spectroscopy studies of carbide derived carbons, Carbon 46 (2008) 1942–1947.
[56] M. Reynaud, J. Serrano-Sevillano, M. Casas-Cabanas, Imperfect battery materials: a closer look at the role of defects in electrochemical performance, Chem. Mater. 35 (2023) 3345–3363.
[57] H.S. Magar, R.Y.A. Hassan, A. Mulchandani, Electrochemical impedance spectroscopy (EIS): principles, construction, and biosensing applications, Sensors 21 (2021) 6578.
[58] L. Zhang, Y. Dai, C. Li, Y. Dang, R. Zheng, Z. Wang, et al., Recent advances in electrochemical impedance spectroscopy for solid-state batteries, Energy Storage Mater. 69 (2024) 103378.
[59] M. Zhang, H. Du, Z. Wei, X. Zhang, R. Wang, Facile electrodeposition of Mn-CoP nanosheets on Ni foam as high-rate and ultrastable electrodes for supercapacitors, ACS Appl. Energy Mater. 5 (2022) 186–195.
[60] S. Schenker, S. Handschin, B. Frey, R. Perren, F. Escher, Pore structure of coffee beans affected by roasting conditions, J. Food Sci. 65 (2000) 452–457.
[61] T. Virtanen, G. Rudolph, A. Lopatina, B. Al-Rudainy, H. Schagerlöf, L. Puro, et al., Analysis of membrane fouling by Brunauer-Emmett-Teller nitrogen adsorption/desorption technique, Sci. Rep. 10 (2020) 3427.
[62] Z. Liu, Y. Zhong, Y. Qiu, L. Cui, W. Yang, J.M. Razal, et al., Multilayered and hierarchical structured NiCo double hydroxide nanosheets generated on porous MgCo2O4 nanowire arrays for high performance supercapacitors, Appl. Surf. Sci. 546 (2021) 149133.
[63] N. Dwivedi, R.J. Yeo, N. Satyanarayana, S. Kundu, S. Tripathy, C.S. Bhatia, Understanding the role of nitrogen in plasma-assisted surface modification of magnetic recording media with and without ultrathin carbon overcoats, Sci. Rep. 5 (2015) 7772.
[64] Z. Zhang, M. Hu, B. Lv, J. Kang, J. Tang, Z. Fei, et al., Solvent-assisted stepwise redox approach to generate zeolite NaA-supported K2O as strong base catalyst for michael addition of ethyl acrylate with ethanol, ACS Omega 3 (2018) 10188–10197.
[65] Y. Liu, Y. Li, F. Li, Y. Liu, X. Yuan, L. Zhang, et al., Conversion of Ti2AlC to C-K2Ti4O9 via a KOH assisted hydrothermal treatment and its application in lithium-ion battery anodes, Electrochim. Acta 295 (2019) 599–604.
[66] J. Lian, L. Xiong, R. Cheng, D. Pang, X. Tian, J. Lei, et al., Ultra-high nitrogen content biomass carbon supercapacitors and nitrogen forms analysis, J. Alloy. Compd. 809 (2019) 151664.
[67] N. Murugan, S. Thangarasu, G.B. Choi, J. Choi, T.H. Oh, Y.A. Kim, Interconnected hierarchical nanoarchitectonics of porous carbon nanosheets derived from renewable biomass for efficient oxygen evolution reaction, J. Alloy. Compd. 923 (2022) 166321.
[68] Z. Guo, J. Zhang, H. Liu, Ultra-high Rhodamine B adsorption capacities from an aqueous solution by activated carbon derived from Phragmites australis doped with organic acid by phosphoric acid activation, RSC Adv. 6 (2016) 40818–40827.
[69] H.-M. Chen, W.-M. Lau, D. Zhou, Waste-coffee-derived activated carbon as efficient adsorbent for water treatment, Materials (2022).
[70] J. Choi, C. Zequine, S. Bhoyate, W. Lin, X. Li, P. Kahol, et al., Waste coffee management: deriving high-performance supercapacitors using nitrogen-doped coffee-derived carbon, C (2019).
[71] D. Lee, Y.-G. Cho, H.-K. Song, S.-J. Chun, S.-B. Park, D.-H. Choi, et al., Coffee-driven green activation of cellulose and its use for all-paper flexible supercapacitors, ACS Appl. Mater. Interfaces 9 (2017) 22568–22577.
[72] Y. Li, B. Qi, Secondary utilization of jujube shell bio-waste into biomass carbon for supercapacitor electrode materials study, Electrochem. Commun. 152 (2023) 107512.
[73] F. Chen, C. Chen, Q. Hu, B. Xiang, T. Song, X. Zou, et al., Synthesis of CuO@CoNi LDH on Cu foam for high-performance supercapacitors, Chem. Eng. J. 401 (2020) 126145.
[74] I.B. Mansir, P.C. Okonkwo, Component degradation in lithium-ion batteries and their sustainability: a concise overview, Sustainability 17 (2025) 1000.
[75] J. Chen, Z. Yan, G. Wang, Y. Ding, M. Xiang, Z. Xu, Hierarchical Ni(OH)2/Cu7S4@CuO heterostructure with enhanced conductivity for efficient hybrid supercapacitor, J. Alloy. Compd. 968 (2023) 171841.
[76] G.Z. Chen, Linear and non-linear pseudocapacitances with or without diffusion control, Prog. Nat. Sci Mater. Int. 31 (2021) 792–800.
[77] S. Waseem, P. Dubey, M. Singh, S. Sundriyal, P.H. Maheshwari, Chemically oxidized carbon paper as a free-standing electrode for supercapacitor: an insight into surface and diffusion contribution, ChemistrySelect 8 (2023) e202204377.
[78] S. Zhu, H. Tao, Y. Liu, X. Ma, K. Wang, Y. Wang, Effect of intrinsic pore distribution on ion diffusion kinetics of supercapacitor electrode surface, J. Phys. Chem. B 126 (2022) 10913–10921.